

Article

# Graphene Embedded with Transition Metals for Capturing Carbon Dioxide: Gas Detection Study Using QM Methods

Fatemeh Mollaamin <sup>1,\*</sup> and Majid Monajjemi <sup>2</sup> 

<sup>1</sup> Department of Biomedical Engineering, Faculty of Engineering and Architecture, Kastamonu University, Kastamonu 37100, Turkey

<sup>2</sup> Department of Chemical Engineering, Central Tehran Branch, Islamic Azad University, Tehran P.O. Box 1496969191, Iran

\* Correspondence: smollaamin@gmail.com

**Abstract:** Carbon dioxide (CO<sub>2</sub>) adsorption on decorated graphene (GR) sheets with transition metals (TMs) including iron, nickel and zinc was investigated for removing this hazardous gas from the environment. TM-doped GR results in higher activity toward gas detecting than pristine graphene nanosheets. TM embedding restrains hydrogen evolution on the C sites, leaving more available sites for a CO<sub>2</sub> decrease. The Langmuir adsorption model with ONIOM using CAM-B3LYP functional and LANL2DZ and 6-31+G (d,p) basis sets due to Gaussian 16 revision C.01 program on the complexes of CO<sub>2</sub>→(Fe, Ni, Zn) embedded on the GR was accomplished. The changes of charge density illustrated a more considerable charge transfer for Zn-embedded GR. The thermodynamic results from IR spectroscopy indicated that  $\Delta G_{\text{ads,CO}_2 \rightarrow \text{Zn@C-GR}}^{\circ}$  has the notable gap of Gibbs free energy adsorption with a dipole moment which defines the alterations between the Gibbs free energy of the initial compounds ( $\Delta G_{\text{CO}_2}^{\circ}$  and  $\Delta G_{\text{Zn@C-GR}}^{\circ}$ ) and product compound ( $\Delta G_{\text{CO}_2 \rightarrow \text{Zn@C-GR}}^{\circ}$ ) through polarizability. Frontier molecular orbital and band energy gaps accompanying some chemical reactivity parameters represented the behavior of molecular electrical transport of the (Fe, Ni, Zn) embedding of GR for the adsorption of CO<sub>2</sub> gas molecules. Our results have provided a favorable understanding of the interaction between TM-embedded graphene nanosheets and CO<sub>2</sub>.

**Keywords:** graphene nanosheet; gas sensor; CO<sub>2</sub>; (Fe, Ni, Zn); environmental pollutant; Langmuir adsorption; DFT



**Citation:** Mollaamin, F.; Monajjemi, M. Graphene Embedded with Transition Metals for Capturing Carbon Dioxide: Gas Detection Study Using QM Methods. *Clean Technol.* **2023**, *5*, 403–417. <https://doi.org/10.3390/cleantechnol5010020>

Academic Editors: Yifan Gu and Zaoming Wang

Received: 31 January 2023

Revised: 6 February 2023

Accepted: 7 March 2023

Published: 9 March 2023



**Copyright:** © 2023 by the authors. Licensee MDPI, Basel, Switzerland. This article is an open access article distributed under the terms and conditions of the Creative Commons Attribution (CC BY) license (<https://creativecommons.org/licenses/by/4.0/>).

## 1. Introduction

The surface of carbon nanostructures is a privileged factor for gas detecting and adsorbing gas devices [1–6].

In addition, enough implanting of the compounds with transition metals might enhance their adsorbing ability and adjust their adsorbing selectivity as the excellent dopant applicants [7–14].

Jayaprakash and coworkers in 2016 have investigated the effect of deficiency on selectivity of nano pristine graphene [15]. They accomplished the DFT method to depict the redox reactivity of pristine and defected graphene surfaces accompanying the rearranging of Stone–Wales and double vacancy deficiencies in their model, which have indicated changes in the bond length of carbon–carbon in the graphene nanosheet [15].

In addition, the outreach of a ReaxFF reactive potential has been studied, which is able to explain the chemistry and dynamics of C-condensed phases using the density functional theory method for achieving the equation of state for graphite and the formation energies of defects in graphene [16]. These calculations were applied to rearrange the parameters of ReaxFFCHO towards a new potential surface as ReaxFFC-2013 based on the DFT method for Stone–Wales transformations in carbon structures [16].

Sensing and grabbing toxic and harmful gases like CO, CO<sub>2</sub>, NO, N<sub>2</sub>O, CH<sub>4</sub>, SO<sub>2</sub> and H<sub>2</sub>S can largely help maintain human health and the ecosystem [17–20].

There are different usages of carbon nanocompounds, such as the adsorbing of hydrogen, hazardous compounds, gas and designing the sensor instruments [21–26].

Recently, many materials including carbon structures have been designed and applied for the adsorptive removal of environmental pollutant gases [27–29]. Thus, it is essential to make high-implement gas detectors for distinguishing these compounds [30,31].

Thus, this research wants to investigate the adsorption of hazardous gases of CO<sub>2</sub> on the carbon nanographene which has been decorated by transition metals of iron, nickel, zinc, manganese, cobalt, and copper, respectively, using a DFT (density functional theory) approach to discover the adsorbing parameters of the various TM-embedded nanographene surfaces.

## 2. Materials and Methods

### 2.1. Adsorptive Removal of Toxic Gases

This article brings up the adsorbing of CO<sub>2</sub> onto transition-metals-embedded carbon nanographene. This part defines the first process of bond formation arising during CO<sub>2</sub> chemisorption and runs over the consequences gained for adsorbing of CO<sub>2</sub> onto the (Fe, Ni, Zn) embedding of carbon nanographene. The resulted data from transition-metal-embedded graphene surface is measured for two toxic gases. Bonding of the CO<sub>2</sub> gas molecules to a TM atom on the GR surface can be observed, as first launched by the giving of the lone pair on the C-atom to the unoccupied d orbitals of the TM atom. The donor potency of CO<sub>2</sub> in this procedure is recognized as being much smaller, and the stability of the TM-C bond is confirmed to be captured by the back donation of electrons from occupied d orbitals on the metal into unoccupied antibonding π\* orbitals on the CO<sub>2</sub> gas molecules. It is assumed that the two steps, donation and back donation, intend to augment each other in a cooperative state.

### 2.2. Langmuir Adsorption Model and Charge Density Analysis

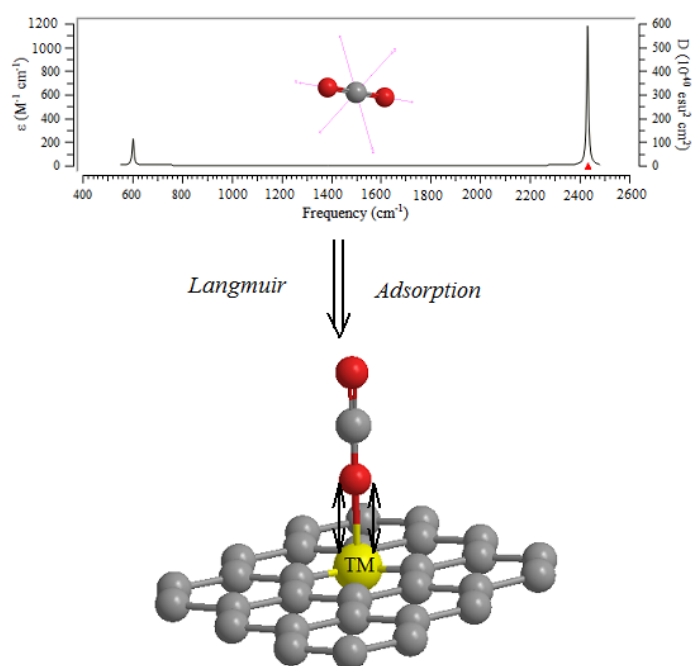
Langmuir adsorbing can be defined through a physical and chemical interaction on the area of the resembling solid state that adsorbs compounds without any interactions with each other, making a mono layer of particles on the solid-state surface.

The Langmuir adsorption equation is the following [32]:

$$\theta_A = \frac{V}{V_m} = \frac{K_{eq}^A p_A}{1 + K_{eq}^A p_A} \quad (1)$$

where  $\theta_A$  is the fractional occupancy of the adsorbing sites; the ratio of  $V$ , the volume of adsorbed gas onto the solid, to  $V_m$ , the volume of a monolayer gas particles coating the entire of the solid surface and totally filled by the adsorbate particle;  $K_{eq}^A$  is the equilibrium constant and  $p_A$  is the adsorbate's partial pressure. A continuing monolayer of adsorbate particles coating a resembling solid surface is the basic concept for this adsorbing system [33–37].

Different studies have concentrated on the gas-adsorbing susceptibilities of C-nanosurfaces which denote a good accord with the Langmuir adsorbing template. The adsorption of toxic NO gas on the Mn-embedded, Co-embedded and Cu-embedded graphene nanosheets has been approved by the most appropriate Langmuir isotherm, which indicates the nature of chemisorption for the bond distance between :  $\ddot{O} = C = \ddot{O}$  and :  $\ddot{O} : - N . = \ddot{O} :$  molecules and TM-embedded C-nanographene, the equilibrium electron diffusion of the adsorbed particles between the solid and gas phases, and a monolayer feature. The gas molecules of :  $\ddot{O} = C = \ddot{O}$  and :  $\ddot{O} : - N . = \ddot{O} :$  are kept on TM-embedded C-nanographene with Langmuir chemisorption (Scheme 1).



**Scheme 1.** IR spectra of  $\text{:}\ddot{\text{O}}=\text{C}=\ddot{\text{O}}$  molecules which adsorb on transition metal (TM) embedding of C-nanographene.

In fact, the mechanism of the gas-sensing phenomenon in the (Fe, Ni, Zn) embedding of C-nanographene would be due to charge transfer between the surface and  $\text{CO}_2$  molecules adsorbed. The changes of charge density analysis in the adsorption process have illustrated that Fe-embedded, Ni-embedded and Zn-embedded C-nanographene show the Mulliken charge of  $-1.345$ ,  $-2.087$  and  $-1.416$ , respectively, before the adsorption of carbon dioxide, and  $-1.898$ ,  $-1.763$  and  $-3.221$ , respectively, after the adsorption of carbon dioxide (Figure 1 and Table 1).

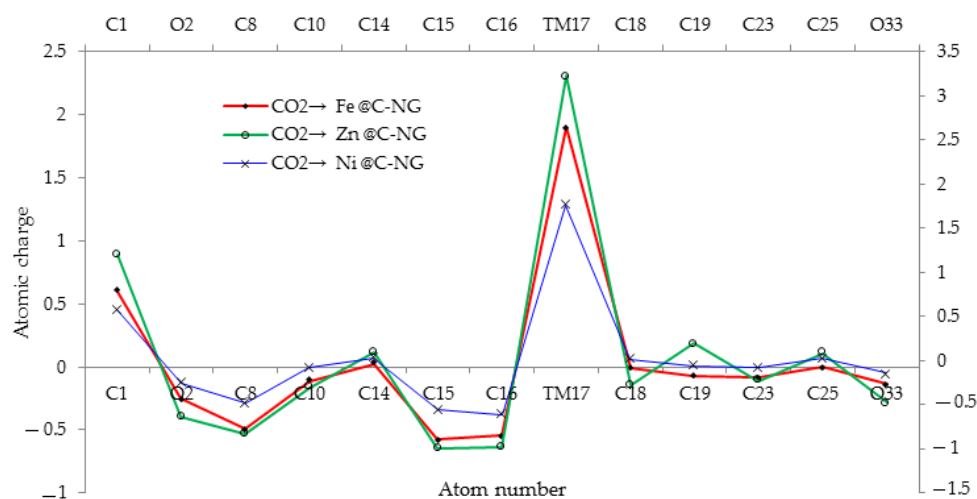


**Figure 1.** The fluctuation of charge distribution versus atom number for adsorbing  $\text{CO}_2$  on the (Fe, Ni, Zn)@C-GR.

**Table 1.** Calculated NMR chemical shielding tensors and Mullikan charge (Q) for some atoms in the active site of CO<sub>2</sub> gas adsorption on the (Fe, Ni, Zn)-embedded C-nanographene.

CO <sub>2</sub> →Fe @C- GR				CO <sub>2</sub> →Ni@C- GR				CO <sub>2</sub> →Zn@C- GR			
Atom	σ <sub>iso</sub>	σ <sub>aniso</sub>	Q	Atom	σ <sub>iso</sub>	σ <sub>aniso</sub>	Q	Atom	σ <sub>iso</sub>	σ <sub>aniso</sub>	Q
C1	148.52	196.31	0.5999	C1	178.24	145.52	0.5848	C1	123.10	234.73	1.1957
O2	321.65	183.04	−0.2528	O2	398.64	64.18	−0.2501	O2	295.29	190.97	−0.6366
C8	100.76	347.30	−0.4878	C8	296.58	574.94	−0.4852	C8	273.90	3225.40	−0.8329
C10	237.59	173.64	−0.1115	C10	41.45	461.74	−0.0808	C10	292.83	1382.14	−0.3038
C14	240.60	485.27	0.0250	C14	68.33	371.25	0.0338	C14	463.91	927.12	0.0904
C15	237.40	341.12	−0.5742	C15	94.84	252.27	−0.5501	C15	534.07	1981.05	−0.9951
C16	183.26	383.67	−0.5461	C16	25.48	160.68	−0.6144	C16	1163.51	3304.01	−0.9772
Fe 17	21,368.96	19,790.99	1.8981	Ni17	7265.00	43,068.15	1.7629	Zn 17	1374.46	528.33	3.2211
C18	40.19	130.77	−0.0049	C18	304.39	798.78	0.0153	C18	233.95	593.95	−0.2791
C19	739.86	1981.10	−0.0750	C19	1620.91	4749.68	−0.0591	C19	5571.71	12,698.28	0.1942
C23	93.25	179.03	−0.0816	C23	68.71	216.09	−0.0767	C23	127.04	228.84	−0.2287
C25	267.56	385.81	0.0005	C25	130.48	138.07	0.0295	C25	630.19	1178.08	0.0828
O33	284.15	153.28	−0.1321	O33	343.76	111.69	−0.1407	O33	293.15	160.22	−0.4784

The chemical shielding (CS) tensors in principal axes system evaluate the isotropic chemical shielding ( $\sigma_{\text{iso}}$ ), anisotropic chemical shielding ( $\sigma_{\text{aniso}}$ ) [38]:  $\sigma_{\text{iso}} = \frac{\sigma_{11} + \sigma_{22} + \sigma_{33}}{3}$ ,  $\sigma_{\text{aniso}} = -\frac{\sigma_{11} + \sigma_{22}}{2} + \sigma_{33}$ .

Therefore, the changes of charge density for the Langmuir adsorption of carbon dioxide on Fe-embedded, Ni-embedded, and Zn-embedded C-nanographene alternatively are  $|\Delta Q_{\text{Zn-doped}}| = -1.805 \gg |\Delta Q_{\text{Fe-doped}}| = -0.553 \gg |\Delta Q_{\text{Ni-doped}}| = +0.324$  (Figure 1 and Table 1). The values of the changes of charge density have illustrated a more significant charge transfer for Zn-embedded C-nanographene.

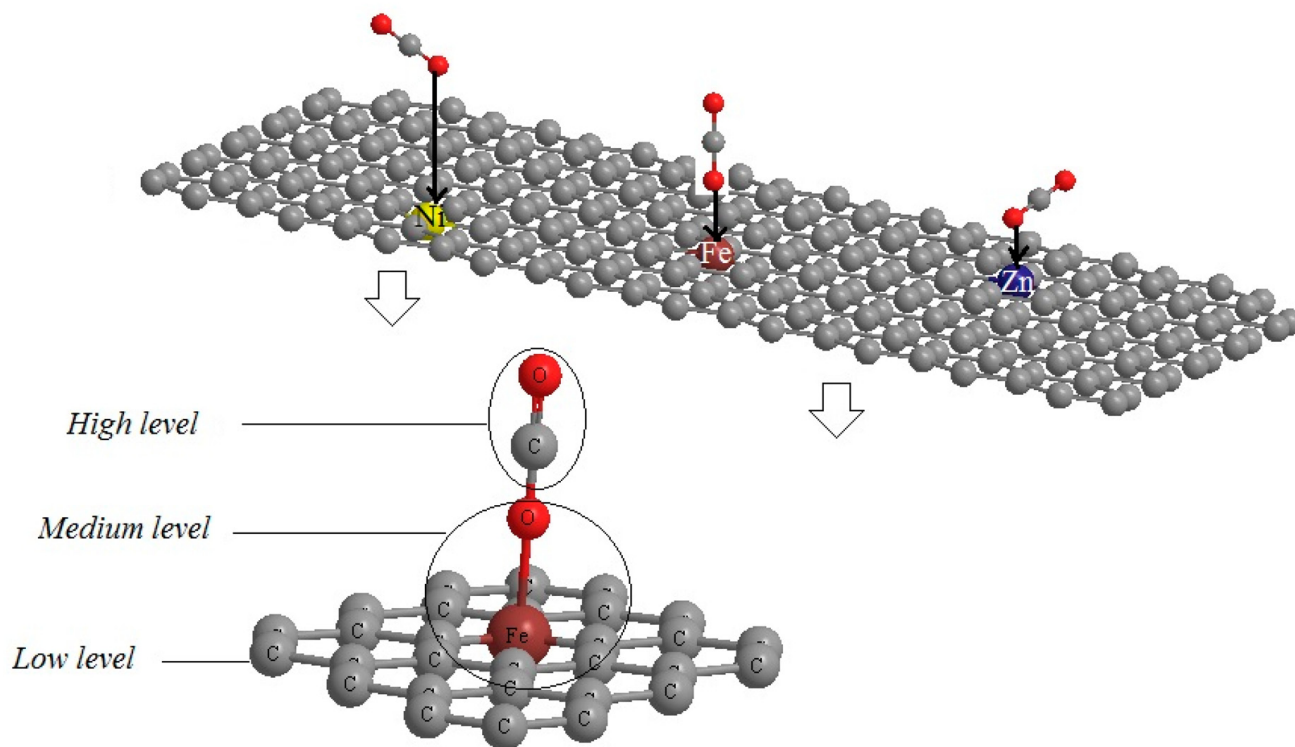
### 2.3. ONIOM Model

Our own n-layered Integrated molecular Orbital and Molecular mechanics, or ONIOM, merges three theoretical levels that are combined for reducing the sequence of validity as the high, medium and low degrees of theory. In this model, a high-degree level has been performed using the density functional theory insight of the CAM-B3LYP functional, which merges the hybrid qualities of B3LYP and the correction of long-range term [39] with a 6-31+G (d,p) basis set [40] for some carbon atoms in nanographene and oxygen atoms in the adsorption zone, and an EPR-III basis set for nitrogen and LANL2DZ for some iron, nickel, zinc, manganese, cobalt and copper atoms through adsorbing CO<sub>2</sub> in the adsorption zone. A medium-degree level has been considered on the other carbon atoms of nanographene in the adsorption zone owing to semi-empirical methodologies. At last, a low-degree level has been depicted on the other iron, nickel, zinc, manganese, cobalt and copper atoms through adsorption of CO<sub>2</sub> with MM2 force fields of molecular mechanic methods  $E_{\text{ONIOM}} = E_{\text{High}} + E_{\text{Medium}} + E_{\text{Low}}$ , (Scheme 2) [41].

In other words, the three-degree model of ONIOM leads to exploring a ground order more precisely than the one-degree model, which might treat a medium-sized order exactly as a huge order with admissible validity [42].

In this article, the structures have been computed using CAM-DFT method on the mechanisms of adsorption of CO<sub>2</sub> by the (Fe, Ni, Zn) embedding of C-nanographene through bonding between transition metals and gas molecules. It has been discovered that the surface binding zone preference of O-atoms of CO<sub>2</sub> in an adsorption zone are greatly influenced by the existence of neighboring atoms in the C-nanographene. The calculated pair distribution functions in the CO<sub>2</sub>→Fe/Ni/Zn embedding of C- GR has depicted that the creation of complexes leads to shorter bond lengths of O→Fe (1.90 Å), O→Ni (1.88 Å) and O→Zn (1.98 Å), once balanced to the analogous increment. Furthermore, the graphene sheet has been optimized and the C–C bond length in GR has been calculated at about 1.42 Å, which has the appropriate accord with the experimental amount (Scheme 2) [43].

After the doping of TM on the graphene sheet, the bond length of Fe–C was 2.29 Å, O→Ni, 2.01 Å and Zn–C, 2.33 Å, which was larger than corresponding bond length of the TM–TM atom in the mass.



**Scheme 2.** Langmuir adsorbing of CO<sub>2</sub> as the toxic gas pollutant onto (Fe, Ni, Zn) embedding of C-nanographene graphene on optimized structure due to three-degree layered of high, medium and low levels of ONIOM model.

The transition-metal-embedded graphene sheet has been made by a hard system and Z-Matrix format of which a blank line has been positioned. The hard potential energy surface has been exposed at a CAM-B3LYP functional [44,45], and concerns LANL2DZ/6-31+ G (d,p) basis sets to appoint frontier molecular orbital, Mulliken charges, nuclear magnetic resonance properties, dipole moment, thermodynamic characteristics and other quantum attributes [46]. In this research, CO<sub>2</sub> molecules have been adsorbed onto TM-embedded C-nanographene toward the formation of CO<sub>2</sub>→Fe/Ni/Zn embedding of C-GR sheets using Gaussian 16 revision C.01 software [47]. This software is applied for molecular designing, causing automated scientific sequences to simplify more fast and extensive quantum chemistry computations [47].

### 3. Results

Based on the computational results, transition metals of manganese, iron, cobalt, nickel, copper and zinc embedded on the nanographene have been investigated as efficient surfaces for the adsorption toxic gas of carbon dioxide (CO<sub>2</sub>) causing air pollution. These experiments have been accomplished using spectroscopy analysis through some physico-chemical attributes.

#### 3.1. NMR Spectra

The analysis of altering in magnetic properties of surfaces upon interaction with gases can be an appropriate route for detecting the gases [48–50]. In fact, the application of magnetic attributes can be replaced with electrical parameters changes owing to the interaction between graphene nanosheet and CO<sub>2</sub> molecules.

Concerning nuclear magnetic resonance spectroscopy, parameters of isotropic ( $\sigma_{\text{iso}}$ ) and anisotropy ( $\sigma_{\text{aniso}}$ ) shielding tensors of NMR spectroscopy for certain atoms in the active site of CO<sub>2</sub> adsorption on the (Fe, Ni, Zn)-embedded carbon nanographene, through the creation of the binding between gas molecules and the solid surface, have been evaluated using Gaussian 16 revision C.01 software [47] and represented in Table 1.

The fluctuation of the magnetic properties of a GR nanosheet doped with transition metals persuades a frequency shielding in the magnetostatic surface wave oscillator that can be ascribable in the existence of various gases.

Considering Table 1, the degeneracy of NMR graphs via chemical shielding (ppm) for CO<sub>2</sub> adsorption on the (Fe, Ni, Zn)-embedded carbon nanographene has been depicted. The data of NMR spectroscopy in Table 1 shows approximately the identical chemical shielding behavior of isotropic and anisotropy parameters for CO<sub>2</sub> → Fe @C- GR and CO<sub>2</sub> → Ni @C- GR embedding on the surface of nanographene, respectively.

Therefore, following the changes of magnetic attributes of the graphene sheet doped with transition metals after CO<sub>2</sub> adsorption, the TM-doped GR surface can be applied as an appropriately selective magnetic gas sensor CO<sub>2</sub> detector.

### 3.2. Natural Bond Orbital (NBO) Analysis

Natural bond orbital (NBO) analysis has been employed to investigate the intermolecular and intra-molecular interactions [51] occurring from chemical bonds in the discussed model.

Therefore, NBO analysis of the CO<sub>2</sub> adsorbed on the (Fe, Ni, Zn)-embedded carbon nanographene has illustrated the character of electronic conjugation between bonds in the gas molecules and TM-doped C- GR (Table 2 and Figure 2).

**Table 2.** NBO analysis for adsorbing CO<sub>2</sub> on the (Fe, Ni, Zn)@C- GR and (Mn, Co, Cu)@C- GR, respectively.

NO→TM-Embedded/Gr Nanosheet	Bond Orbital	Occupancy	Hybrids
:Ö = C = Ö : →Fe @C- GR	BD (1) C1–O2	1.9895	0.6388 (sp <sup>1.03</sup> ) C + 0.7694 (sp <sup>3.01</sup> ) O
	BD (1) C1–O3	1.9975	0.6503 (sp <sup>0.97</sup> ) C + 0.7597 (sp <sup>2.93</sup> ) O
	BD (1) C8–Fe17	1.9573	0.8077 (sp <sup>1.70</sup> ) C + 0.5895 (sp <sup>0.31</sup> d <sup>3.23</sup> ) Fe
	BD (1) C15–Fe17	1.9528	0.8178 (sp <sup>1.40</sup> ) C + 0.5756 (sp <sup>0.36</sup> d <sup>3.29</sup> ) Fe
	BD (1) C16–Fe17	1.9613	0.8196 (sp <sup>1.46</sup> ) C + 0.5730 (sp <sup>0.4</sup> d <sup>4.24</sup> ) Fe
:Ö = C = Ö : →Ni @C- GR	BD (1) C1–O2	1.9894	0.6430 (sp <sup>1.02</sup> ) C + 0.7659 (sp <sup>3.25</sup> ) O
	BD (1) C1–O3	1.9974	0.6498 (sp <sup>0.98</sup> ) C + 0.7601 (sp <sup>2.91</sup> ) O
	BD (1) C8–Ni17	1.9682	0.8015 (sp <sup>1.58</sup> ) C + 0.5980 (sp <sup>0.34</sup> d <sup>1.91</sup> ) Ni
	BD (1) C15–Ni17	1.9682	0.8098 (sp <sup>1.38</sup> ) C + 0.5868 (sp <sup>0.38</sup> d <sup>2.13</sup> ) Ni
	BD (1) C16–Ni17	1.9745	0.8219 (sp <sup>1.44</sup> ) C + 0.5697 (sp <sup>0.67</sup> d <sup>4.65</sup> ) Ni
:Ö = C = Ö : →Zn @C- GR	BD (1) C1–O2	1.9948	0.5712 (sp <sup>0.99</sup> ) C + 0.8208 (sp <sup>1.51</sup> ) O
	BD (1) C1–O3	1.9979	0.5802 (sp <sup>1.02</sup> ) C + 0.8145 (sp <sup>1.50</sup> ) O
	BD (1) C8–Zn17	1.9643	0.6481 (sp <sup>1.39</sup> ) C + 0.7616 (sp <sup>0.37</sup> d <sup>2.47</sup> ) Zn
	BD (1) C15–Zn17	1.9592	0.7035 (sp <sup>1.19</sup> ) C + 0.7107 (sp <sup>0.33</sup> d <sup>3.15</sup> ) Zn
	BD (1) C16–Zn17	1.9287	0.7038 (sp <sup>1.25</sup> ) C + 0.7104 (sp <sup>0.62</sup> d <sup>4.67</sup> ) Zn

In Figure 2, it has been observed the fluctuation of occupancy of natural bond orbitals for CO<sub>2</sub>→Fe@C- GR, CO<sub>2</sub>→Ni@C- GR, CO<sub>2</sub>→Zn@C- GR surfaces through the Langmuir adsorption process by indicating the active oxygen atom in carbon dioxide becoming close to the nanographene.

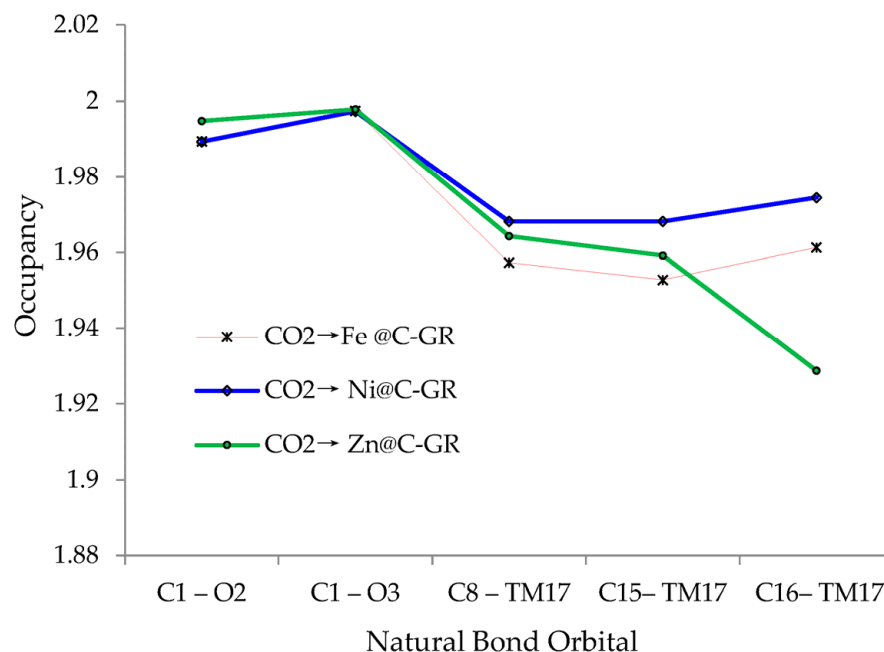


**Figure 2.** Occupancy fluctuation extracted of NBO method for bond lengths of C-O, C-TM (Fe, Ni, Zn) through adsorption of CO<sub>2</sub> TM@C-NG surfaces.

### 3.3. Thermodynamic Properties and IR Spectroscopy Analysis

The capacity of carbon dioxide (CO<sub>2</sub>) adsorption on carbon nanostructures decreases with temperature, which exhibits the exothermic nature of the adsorption process, while the thermodynamic parameters represent low isosteric heats of the adsorption process [52].

Thermodynamic parameters have been estimated due to Gaussian 16 revision C.01 software using CAM-B3LYP/LANL2DZ, 6-31+G (d,p) through for the adsorption of toxic carbon dioxide (: $\ddot{O}$  = C =  $\ddot{O}$  :) on the surfaces of the (Fe, Ni, Zn) embedding of nanographene as the gas sensor which can be used as the selective detectors for environmental hazardous gases (Table 3).

**Table 3.** The thermodynamic attributes of CO<sub>2</sub> adsorbed on the (Fe, Ni, Zn)@C- GR as the selective gas sensor.

Compound	$\Delta E^{\circ} \times 10^{-4}$ (kcal/mol)	$\Delta H^{\circ} \times 10^{-4}$ (kcal/mol)	$\Delta G^{\circ} \times 10^{-4}$ (kcal/mol)	$\Delta G^{\circ}_{ads} \times 10^{-4}$ (kcal/mol)	S <sup>o</sup> (Cal/K.mol)	Dipole Moment (Debye)
: $\ddot{O}$ = C = $\ddot{O}$ :	-11.6121	-11.6121	-11.6136	-	51.378	0.0000
Fe@ C- GR	-146.2783	-146.2782	-146.2816	-	111.175	2.3199
Ni@ C- GR	-162.4794	-162.4793	-162.4828	-	116.150	13.6226
Zn@ C- GR	-178.2031	-178.2030	-178.2066	-	120.533	1.7301
: $\ddot{O}$ = C = $\ddot{O}$ : → Fe @C- GR	-157.8893	-157.8893	-157.8932	0.002	130.634	14.1988
: $\ddot{O}$ = C = $\ddot{O}$ : → Ni @C- GR	-173.0324	-173.0323	-173.0360	1.0604	122.276	12.5830
: $\ddot{O}$ = C = $\ddot{O}$ : → Zn @C- GR	-191.0952	-191.0951	-191.0989	-1.2787	127.012	2.0963

Furthermore, the infrared spectra for the adsorption of CO<sub>2</sub> by (Fe, Ni, Zn) embedded onto C-nanographene have been reported in Figure 3a–c.

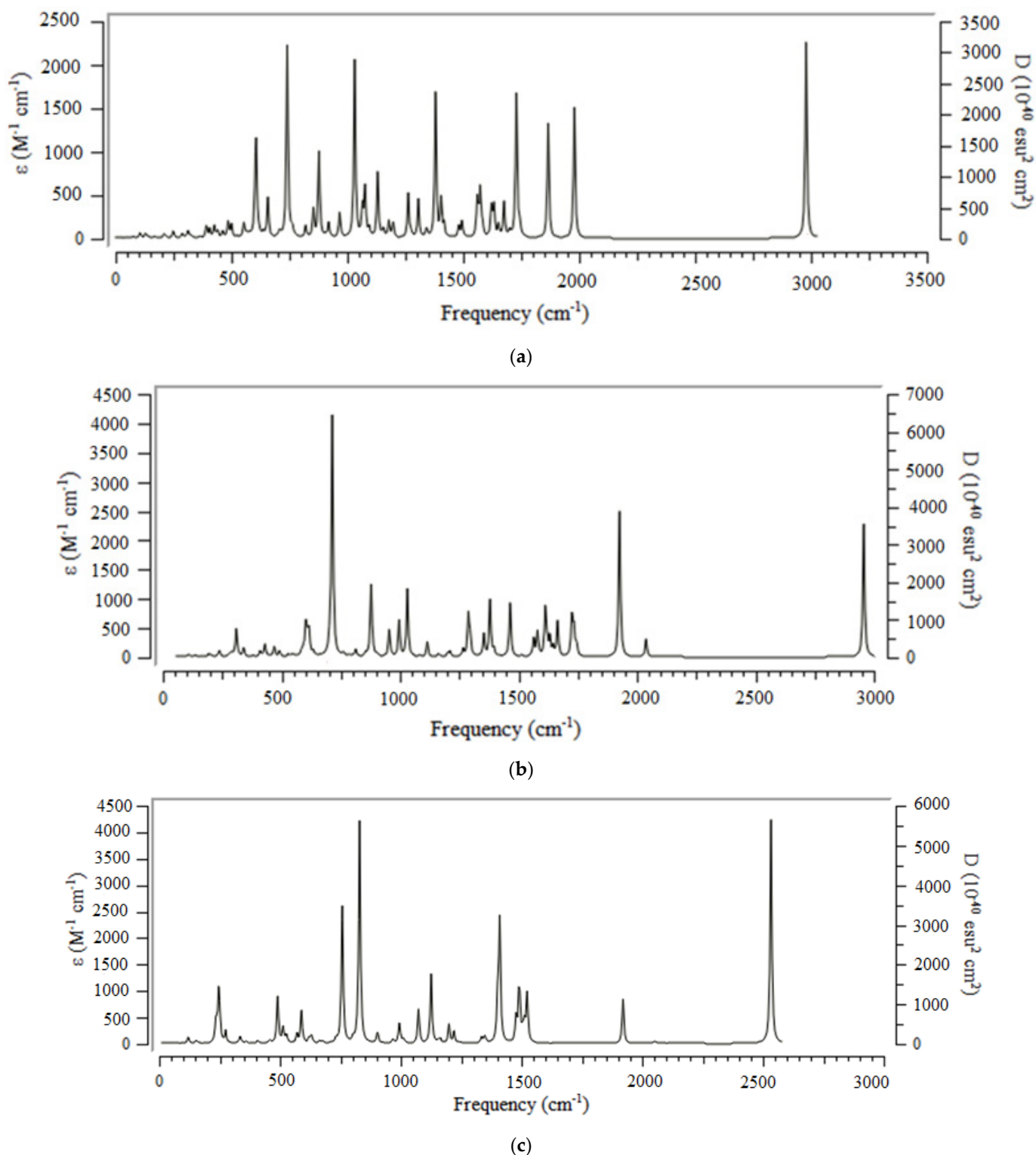


**Figure 3.** Alterations of frequency ( $\text{cm}^{-1}$ ) in the IR spectra for (a)  $:\ddot{\text{O}}=\text{C}=\ddot{\text{O}}: \rightarrow \text{Fe} @\text{C}-\text{GR}$ , (b)  $:\ddot{\text{O}}=\text{C}=\ddot{\text{O}}: \rightarrow \text{Ni} @\text{C}-\text{GR}$ , (c)  $:\ddot{\text{O}}=\text{C}=\ddot{\text{O}}: \rightarrow \text{Zn} @\text{C}-\text{GR}$  as the selective gas sensors.

The graphs of  $:\ddot{\text{O}}=\text{C}=\ddot{\text{O}}: \rightarrow \text{Fe} @\text{C}-\text{GR}$ ,  $:\ddot{\text{O}}=\text{C}=\ddot{\text{O}}: \rightarrow \text{Ni} @\text{C}-\text{GR}$ , and  $:\ddot{\text{O}}=\text{C}=\ddot{\text{O}}: \rightarrow \text{Zn} @\text{C}-\text{GR}$  have shown the frequency range around  $500 \text{ cm}^{-1}$ – $3000 \text{ cm}^{-1}$  with the strongest peaks in IR spectrum around  $750 \text{ cm}^{-1}$  and  $3000 \text{ cm}^{-1}$  Figure 3a–c.

From Figure 4, it could be understood that the maximum of the Langmuir adsorbing isotherm plots related to  $\Delta G_{\text{ads}}^{\circ}$  versus a dipole moment may depend on the interactions

between the CO<sub>2</sub> and TM-embedded C-nanographene. The order of Gibbs free energy changes for clusters of gas→TM@C-GR is  $\Delta G_{\text{CO}_2 \rightarrow \text{Zn@C}}^0 > \Delta G_{\text{CO}_2 \rightarrow \text{Ni@C}}^0 > \Delta G_{\text{CO}_2 \rightarrow \text{Fe@C}}^0$ .

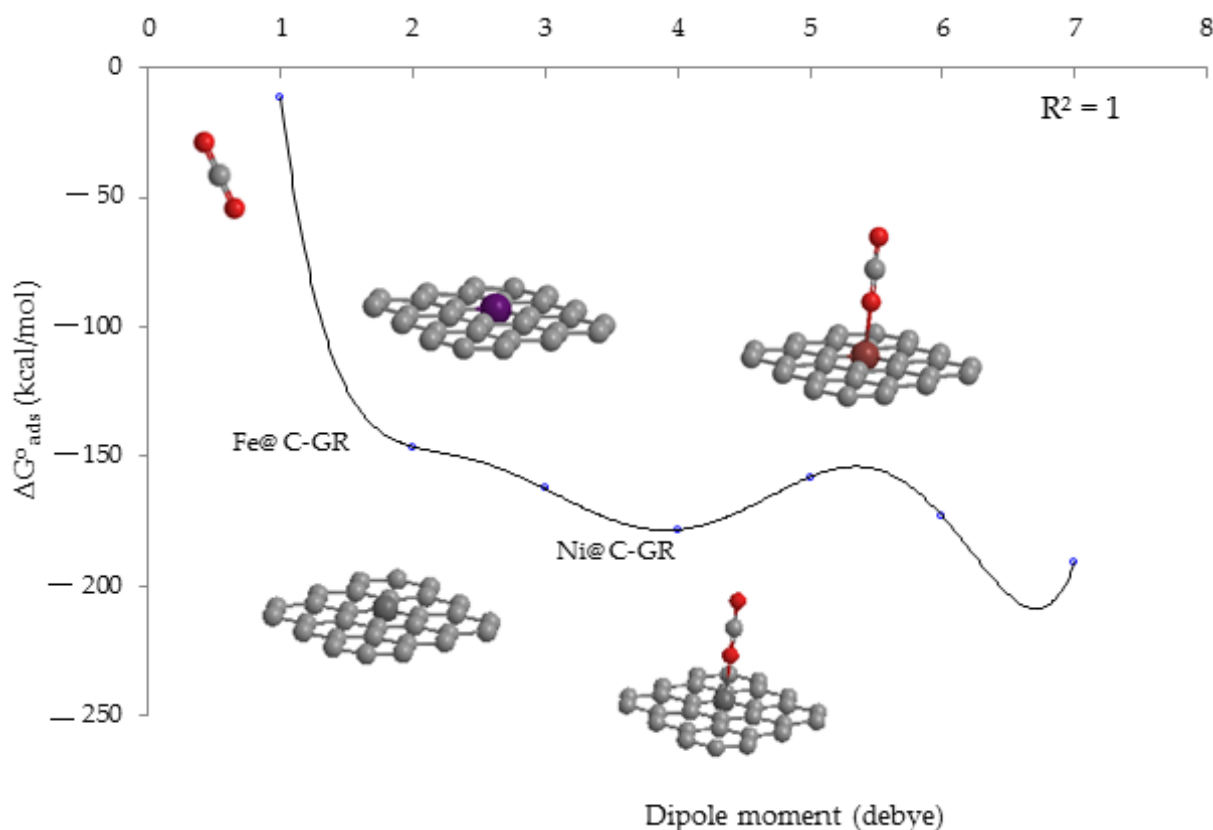


**Figure 4.** The changes of Gibbs free energy (kcal/mol) versus dipole moment (Debye) for adsorption of CO<sub>2</sub> on the (Fe, Ni, Zn) embedding of C-nanographene surfaces.

The change of energy band gaps for the most stable structure of CO<sub>2</sub> molecules adsorbed on the GR sheet doped with TM has been graphed in respect of the corresponding pure sheet due to the thermodynamic reported data in Table 3 (Figure 4).

The adsorptive capacity of CO<sub>2</sub> on the TM-embedded C-nanographene is approved by the  $\Delta G_{\text{ads}}^0$  amounts:

$$\Delta G_{\text{ads,CO}_2 \rightarrow \text{TM@C-GR}}^0 = \Delta G_{\text{CO}_2 \rightarrow \text{TM@C-GR}}^0 - (\Delta G_{\text{CO}_2}^0 + \Delta G_{\text{TM@C-GR}}^0); (\text{TM} = \text{Fe, Ni, Zn}) \quad (2)$$

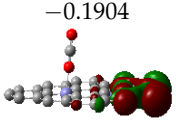
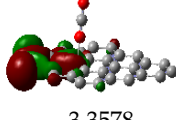
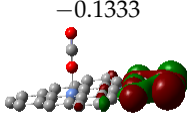
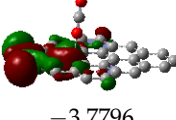
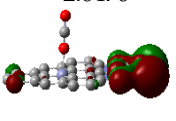
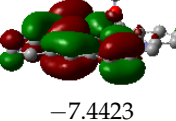
On the basis of data in Table 3, it is predicted that the adsorption of CO<sub>2</sub> on the TM-embedded graphene nanosheet must be physico-chemical attributes. As seen in Figure 4,  $\Delta G_{\text{ads,CO}_2 \rightarrow \text{Zn@C-GR}}^0$  ( $-1.2787 \times 10^4$ , kcal/mol) has the largest gap of Gibbs free energy adsorption with a dipole moment which defines the alterations between the Gibbs free energies of initial compounds ( $\Delta G_{\text{CO}_2}^0$  and  $\Delta G_{\text{Zn@C-GR}}^0$ ) and product compound ( $\Delta G_{\text{CO}_2 \rightarrow \text{Zn@C-GR}}^0$ ) through polarizability. In fact, TM-embedded C-nanographene can possess enough efficiency for the adsorption of the toxic gases carbon dioxide and nitrogen dioxide through charge transfer from oxygen atoms to transition metals.

The electric dipole moments from the computations have been summarized in Table 3. They display that the dipole moment diffused by the transitions metals of Fe, Ni and Zn has been augmented. After the doping of transition metals on the GR nanosheet, the distribution of electrons will influence electric dipole moments, causing long-range interactions between the CO<sub>2</sub> molecules adsorbing on the GR nanosheet concerning the effect of transition metals on the zone growth (Figure 4).

### 3.4. Frontier Molecular Orbital's of HOMO, LUMO and UV-VIS Analysis

The lowest unoccupied molecular orbital (LUMO) energy is generated by ionization and the highest occupied molecular orbital (HOMO) energy is observed by the electron affinity. These parameters have been evaluated for adsorption of carbon dioxide on the (Fe, Ni, Zn) embedding of nanographene as the gas detector in Table 4. The HOMO (ev), LUMO (ev), and band energy gap ( $\Delta E = E_{\text{LUMO}} - E_{\text{HOMO}}$ ) (ev) have exhibited the pictorial explanation of the frontier molecular orbitals and their respective positive and negative areas, which are a significant parameter for discovering the molecular properties of efficient compounds in adsorption of CO<sub>2</sub> on the TM-embedded nanographene surface (Table 4).

**Table 4.** The LUMO (ev), HOMO (ev), band energy gap ( $\Delta E$ /ev) and other qualifications (ev) for adsorption of CO<sub>2</sub> on the (Fe, Ni, Zn) embedding of C-nanographene surfaces using CAM-B3LYP/LANL2DZ, 6-31+G (d,p).

Gas→TM@C- GR	LUMO	HOMO	$\Delta E$	$\mu$	$\chi$	$\eta$	$\zeta$	$\psi$
: $\ddot{\text{O}} = \text{C} = \ddot{\text{O}}$ : →Fe@C- GR	-0.1904 	-3.3578 	3.1666	-1.7748	1.7748	1.5833	0.3158	0.9947
: $\ddot{\text{O}} = \text{C} = \ddot{\text{O}}$ : →Ni@C- GR	-0.1333 	-3.7796 	3.6471	-1.9563	1.9563	1.8235	0.2742	1.0494
: $\ddot{\text{O}} = \text{C} = \ddot{\text{O}}$ : →Zn@C- GR	-2.6476 	-7.4423 	4.7952	-5.0463	5.0463	2.3976	0.2085	5.3105

Moreover, for getting more conclusive approving in identifying the compound characteristics of adsorption complexes of CO<sub>2</sub> on the (Fe, Ni, Zn) embedding of C-nanographene surfaces, a series of chemical reactivity parameters, such as chemical potential ( $\mu$ ), electronegativity ( $\chi$ ), hardness ( $\eta$ ), softness ( $\zeta$ ) and electrophilicity index ( $\psi$ ), have been carried out (Table 4) [53–55].

Figure 5 has drawn that chemical potential ( $\mu$ ) for CO<sub>2</sub> adsorption on the surface of a zinc embedding of carbon-nanographene has a considerable minimum potential well. The negative content of the chemical potential ( $\mu$ ) and the positive contents of other factors have remarked an admissible efficiency of scavenging CO<sub>2</sub> by zinc-embedded carbon-nanographene. In fact, the chemical potential defined the increase of CO<sub>2</sub> molecules to the crystal of Zn@C- GR while the number of other particles and the number of unoccupied lattice locations kept constant. As a matter of fact, enhancement of the gas molecules of CO<sub>2</sub> thus involves the simultaneous increasing of a lattice site or unit cell to the crystal of the Zn@C- GR surface. This procedure leads to an augmentation in surface region and, thereby, energy must be spent in generating a new surface of nanographene. In addition, the alliance of particles alters the mass of the crystal and the process is also accomplished versus the mechanical powers.

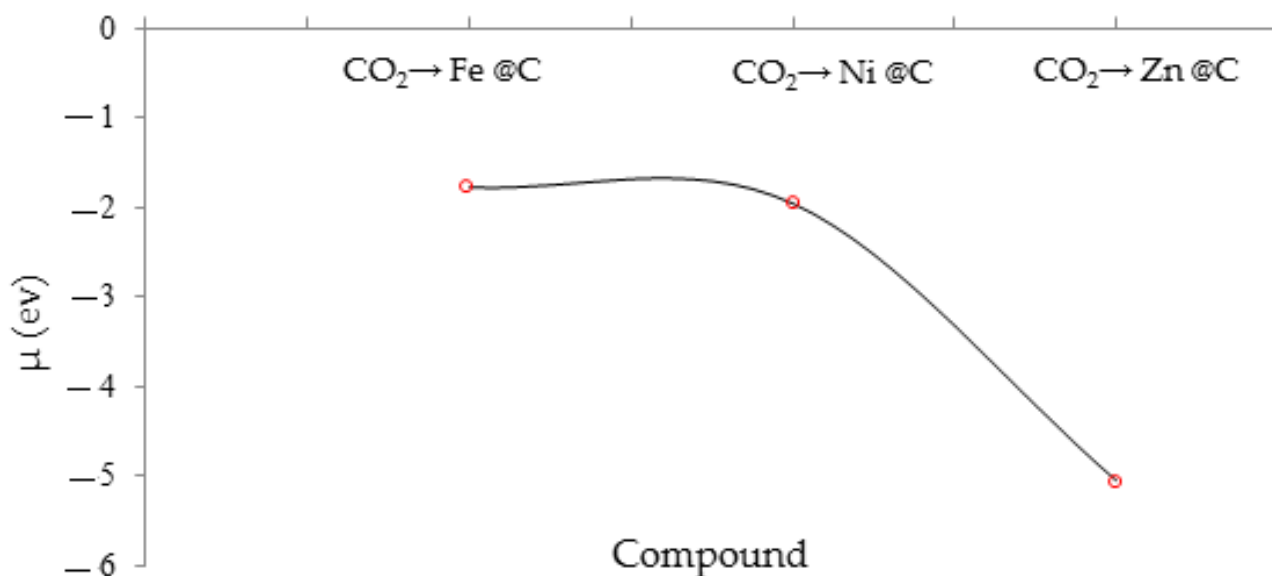


**Figure 5.** The chemical potential ( $\mu$ ) of CO<sub>2</sub> adsorption onto the crystal of Zn@C- GR.

From Table 3, the Zn@C- GR surface has indicated the considerable value of stabilized energy compared to Fe@C- GR and Ni@C- GR. In addition, the parameter of chemical potential ( $\mu$ ) has approved the activity of zinc atoms that might form the bonds with the oxygen atoms of CO<sub>2</sub> from functional groups towards the covalent bond of optimized coordination, performing like grapnel sites for increasing the sensitivity and selectivity of the GR nanosheet (Figure 5).

In this work, the energy gap establishes how toxic gases of CO<sub>2</sub> can be adsorbed on the (Fe, Ni, Zn) embedding of nanographene as the gas sensors with the CAM-B3LYP/LANL2DZ, 6-311+G (2d, p) quantum approach. In addition, frontier molecular orbitals perform an essential function in the optical and electrical factors like ultraviolet and visible spectra [56].

The energy gap between LUMO and HOMO has recognized the qualifications of molecular electrical transport [57].

Furthermore, TD-DFT/LANL2DZ, 6-31+G (d,p) calculations with a CAM-B3LYP functional have been accomplished to discern the low-lying excited states of CO<sub>2</sub> can be adsorbed on the (Fe, Ni, Zn) embedding of nanographene. The consequences contain the vertical stimulation energies, oscillator strength and wavelength, which have been introduced in Figure 6a–c.

Figure 6a–c have shown UV-VIS spectra for CO<sub>2</sub> → Fe @C- GR, CO<sub>2</sub> → Ni @C- GR, CO<sub>2</sub> → Zn @C- GR with maximum adsorption bands between 1000–5000 nm. Moreover, a sharp peak around 2500 nm for CO<sub>2</sub> → TM@C- GR using a CAM-B3LYP functional has been observed (Figure 6a–c).

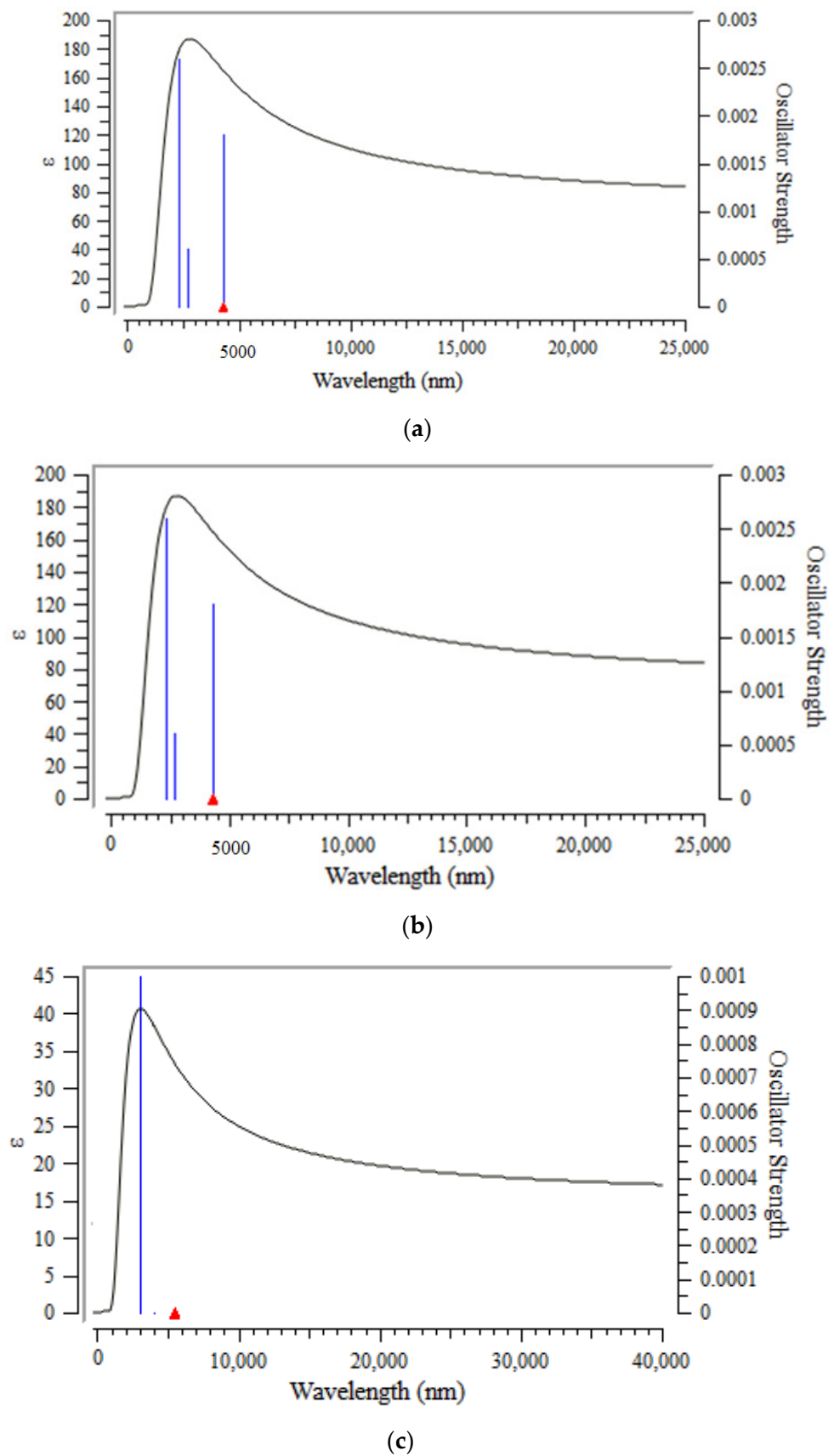


**Figure 6.** UV-VIS spectra for (a) :  $\ddot{O} = C = \ddot{O} : \rightarrow Fe @C- GR$ , (b) :  $\ddot{O} = C = \ddot{O} : \rightarrow Ni @C- GR$ , and (c) :  $\ddot{O} = C = \ddot{O} : \rightarrow Zn @C- GR$  as the selective gas sensors.

#### 4. Conclusions

This article has reported the trends for toxic carbon dioxide (CO<sub>2</sub>) adsorption on transition metals of iron, nickel and zinc embedding of carbon-nanographene surface.

In particular, the energetic, structural and infrared adsorption characteristics of linearly (atop) CO<sub>2</sub> adsorbed on (Fe, Ni, Zn) embedding of C-GR have been discussed. Spin-unrestricted density functional theory (DFT) calculations were applied to verdict the tendency of CO<sub>2</sub> adsorption energy of (CO<sub>2</sub>→Fe-, CO<sub>2</sub>→Ni-, CO<sub>2</sub>→Zn-) embedded on the nanographene sheet and normal mode vibrational frequencies ( $\nu_{\text{CO}_2}$ ) of  $\ddot{\text{O}} = \text{C} = \ddot{\text{O}}$  for clusters composed of Fe, Ni and Zn.

Moreover, the adsorption of CO<sub>2</sub> molecules has indicated the spin polarization in GR nanosheets with a magnetic moment of transition metals, exhibiting that the magnetic properties of the TM-doped GR nanosheet has changed.

The effects of the transition metal electronic structure onto the adsorption energy of CO<sub>2</sub> toxic gas and how these chemical factors might be related to the catalytic activity of transition-supported metal catalysts that deal with adsorption, and surface diffusion, have been investigated.

**Author Contributions:** F.M.: Conceptualization and idea, Methodology, Software, Validation, Formal analysis, Investigation, Data Curation, Writing—original draft preparation, Visualization, Supervision, Project administration. M.M.: Methodology, Software, Formal analysis, Investigation, Data Curation, Writing—review and editing, Visualization, Resources. All authors have read and agreed to the published version of the manuscript.

**Funding:** This research received no external funding.

**Institutional Review Board Statement:** Not applicable.

**Informed Consent Statement:** Not applicable.

**Data Availability Statement:** Not applicable.

**Acknowledgments:** In successfully completing this paper and its research, the authors are grateful to Kastamonu University for their support through the library, the laboratory and scientific websites.

**Conflicts of Interest:** The authors declare no conflict of interest.

#### References

1. Wang, C.; Wang, Z.; Zhang, S.; Zhang, J.; Li, K. Ab Initio Investigation of the Adsorption of CO<sub>2</sub> Molecules on Defect Sites of Graphene Surfaces: Role of Local Vacancy Structures. *Materials* **2023**, *16*, 981. [[CrossRef](#)] [[PubMed](#)]
2. Mihet, M.; Dan, M.; Lazar, M.D. CO<sub>2</sub> Hydrogenation Catalyzed by Graphene-Based Materials. *Molecules* **2022**, *27*, 3367. [[CrossRef](#)]
3. Li, H.; Li, T.; Deng, W.; Kong, S. Preparation and Adsorption Properties of Graphene-Modified, Pitch-Based Carbon Foam Composites. *Polymers* **2022**, *14*, 4455. [[CrossRef](#)] [[PubMed](#)]
4. Fatima, S.S.; Borhan, A.; Ayoub, M.; Ghani, N.A. CO<sub>2</sub> Adsorption Performance on Surface-Functionalized Activated Carbon Impregnated with Pyrrolidinium-Based Ionic Liquid. *Processes* **2022**, *10*, 2372. [[CrossRef](#)]
5. Duan, T.; Li, H.; Daukiya, L.; Simon, L.; Leifer, K. Enhanced Ammonia Gas Adsorption through Site-Selective Fluorination of Graphene. *Crystals* **2022**, *12*, 1117. [[CrossRef](#)]
6. Yang, L.; Xiao, W.; Wang, J.; Li, X.; Wang, L. Adsorption and Sensing Properties of Formaldehyde on Chemically Modified Graphene Surfaces. *Crystals* **2022**, *12*, 553. [[CrossRef](#)]
7. Lisovski, O.; Piskunov, S.; Bocharov, D.; Zhukovskii, Y.F.; Kleperis, J.; Knoks, A.; Lesnicenoks, P. CO<sub>2</sub> and CH<sub>2</sub> Adsorption on Copper-Decorated Graphene: Predictions from First Principle Calculations. *Crystals* **2022**, *12*, 194. [[CrossRef](#)]
8. Yan, H.; Ku, P.-C.; Gan, Z.-Y.; Liu, S.; Li, P. Strain Effects in Gallium Nitride Adsorption on Defective and Doped Graphene: First-Principles Calculations. *Crystals* **2018**, *8*, 58. [[CrossRef](#)]
9. Shahriari, S.; Mollaamin, F.; Monajjemi, M. Increasing the Performance of  $\{(1-x-y) \text{LiCo}_{0.3}\text{Cu}_{0.7}\} (\text{Al and Mg doped}) \text{O}_2\}$ ,  $x\text{Li}_2\text{MnO}_3$ ,  $y\text{LiCoO}_2$  Composites as Cathode Material in Lithium-Ion Battery: Synthesis and Characterization. *Micromachines* **2023**, *14*, 241. [[CrossRef](#)]
10. Peng, S.; Zhang, J.; Jin, Z.; Zhang, D.; Shi, J.; Wei, S. Electric-Field Induced Doping Polarity Conversion in Top-Gated Transistor Based on Chemical Vapor Deposition of Graphene. *Crystals* **2022**, *12*, 184. [[CrossRef](#)]
11. Montejo-Alvaro, F.; Martínez-Espinosa, J.A.; Rojas-Chávez, H.; Navarro-Ibarra, D.C.; Cruz-Martínez, H.; Medina, D.I. CO<sub>2</sub> Adsorption over 3d Transition-Metal Nanoclusters Supported on Pyridinic N<sub>3</sub>-Doped Graphene: A DFT Investigation. *Materials* **2022**, *15*, 6136. [[CrossRef](#)]

12. Liu, X.; Wang, C.-Z.; Hupalo, M.; Lin, H.-Q.; Ho, K.-M.; Tringides, M.C. Metals on Graphene: Interactions, Growth Morphology, and Thermal Stability. *Crystals* **2013**, *3*, 79–111. [[CrossRef](#)]
13. Vinogradov, K.Y.; Bulanova, A.V.; Shafigulin, R.V.; Tokranova, E.O.; Zhu, H. Quantum-Chemical Modeling of the Catalytic Activity of Graphene Doped with Metal Phthalocyanines in ORR. *Catalysts* **2022**, *12*, 786. [[CrossRef](#)]
14. Canales, M.; Ramírez-De-Arellano, J.M.; Arellano, J.S.; Magaña, L.F. Ab Initio Study of the Interaction of a Graphene Surface Decorated with a Metal-Doped C<sub>30</sub> with Carbon Monoxide, Carbon Dioxide, Methane, and Ozone. *Int. J. Mol. Sci.* **2022**, *23*, 4933. [[CrossRef](#)] [[PubMed](#)]
15. Jayaprakash, G.K.; Casillas, N.; Astudillo-Sánchez, P.D.; Flores-Moreno, R. Role of Defects on Regioselectivity of Nano Pristine Graphene. *J. Phys. Chem. A* **2016**, *120*, 9101–9108. [[CrossRef](#)] [[PubMed](#)]
16. Srinivasan, S.G.; van Duin, A.C.T.; Ganesh, P. Development of a ReaxFF Potential for Carbon Condensed Phases and Its Application to the Thermal Fragmentation of a Large Fullerene. *J. Phys. Chem. A* **2015**, *119*, 571–580. [[CrossRef](#)]
17. Su, Y.; Wang, J.; Wang, B.; Yang, T.; Yang, B.; Xie, G.; Zhou, Y.; Zhang, S.; Tai, H.; Cai, Z.; et al. Alveolus-Inspired Active Membrane Sensors for Self-Powered Wearable Chemical Sensing and Breath Analysis. *ACS Nano* **2020**, *14*, 6067–6075. [[CrossRef](#)]
18. Ma, D.; Zhang, J.; Li, X.; He, C.; Lu, Z.; Lu, Z.; Yang, Z.; Wang, Y. C<sub>3</sub>N monolayers as promising candidates for NO<sub>2</sub> sensors. *Sens. Actuators B Chem.* **2018**, *266*, 664–673. [[CrossRef](#)]
19. Pacheco, M.; Pacheco, J.; Valdivia, R.; Santana, A.; Tu, X.; Mendoza, D.; Frias, H.; Medina, L.; Macias, J. Green Applications of Carbon Nanostructures produced by Plasma Techniques. *MRS Adv.* **2017**, *2*, 2647–2659. [[CrossRef](#)]
20. Joel, E.F.; Lujanienė, G. Progress in Graphene Oxide Hybrids for Environmental Applications. *Environments* **2022**, *9*, 153. [[CrossRef](#)]
21. Kroto, H.W.; Heath, J.R.; O'Brien, S.C.; Curl, R.F.; Smalley, R.E. C<sub>60</sub>: Buckminsterfullerene. *Nature* **1985**, *318*, 162–163. [[CrossRef](#)]
22. Nasibulin, A.G.; Pikhitsa, P.V.; Jiang, H.; Brown, D.P.; Krasheninnikov, A.V.; Anisimov, A.S.; Queipo, P.; Moisala, A.; Gonzalez, D.; Lientschnig, G.; et al. A novel hybrid carbon material. *Nat. Nanotechnol.* **2007**, *2*, 156–161. [[CrossRef](#)] [[PubMed](#)]
23. Moisala, A.; Nasibulin, A.G.; Shandakov, S.D.; Jiang, H.; Kauppinen, E.I. On-line detection of single-walled carbon nanotube formation during aerosol synthesis methods. *Carbon* **2005**, *43*, 2066–2074. [[CrossRef](#)]
24. Delgado, J.L.; Herranz, M.; Martín, N. The nano-forms of carbon. *J. Mater. Chem.* **2008**, *18*, 1417–1426. [[CrossRef](#)]
25. Falcao, E.H.; Wudl, F. Carbon allotropes: Beyond graphite and diamond. *J. Chem. Technol. Biotechnol.* **2007**, *82*, 524–531. [[CrossRef](#)]
26. Langenhorst, F.; Campione, M. Ideal and real structures of different forms of carbon, with some remarks on their geological significance. *J. Geol. Soc.* **2018**, *176*, 337–347. [[CrossRef](#)]
27. Lee, S.W.; Lee, W.; Hong, Y.; Lee, G.; Yoon, D.S. Recent advances in carbon material-based NO<sub>2</sub> gas sensors. *Sensors Actuators B Chem.* **2018**, *255*, 1788–1804. [[CrossRef](#)]
28. Chatterjee, S.G.; Chatterjee, S.; Ray, A.K.; Chakraborty, A.K. Graphene–metal oxide nanohybrids for toxic gas sensor: A review. *Sens. Actuators B Chem.* **2015**, *221*, 1170–1181. [[CrossRef](#)]
29. Xiao, Z.; Kong, L.B.; Ruan, S.; Li, X.; Yu, S.; Li, X.; Jiang, Y.; Yao, Z.; Ye, S.; Wang, C.; et al. Recent development in nanocarbon materials for gas sensor applications. *Sens. Actuators B Chem.* **2018**, *274*, 235–267. [[CrossRef](#)]
30. Jayaprakash, G.K. Pre-post redox electron transfer regioselectivity at the alanine modified nano graphene electrode interface. *Chem. Phys. Lett.* **2021**, *789*, 139295. [[CrossRef](#)]
31. Ramirez-De-Arellano, J.M.; Canales, M.; Magaña, L.F. Carbon Nanostructures Doped with Transition Metals for Pollutant Gas Adsorption Systems. *Molecules* **2021**, *26*, 5346. [[CrossRef](#)]
32. Hanaor, D.A.H.; Ghadiri, M.; Chrzanowski, W.; Gan, Y. Scalable Surface Area Characterization by Electrokinetic Analysis of Complex Anion Adsorption. *Langmuir* **2014**, *30*, 15143–15152. [[CrossRef](#)] [[PubMed](#)]
33. Boyd, A.; Dube, I.; Fedorov, G.; Paranjape, M.; Barbara, P. Gas sensing mechanism of carbon nanotubes: From single tubes to high-density networks. *Carbon* **2014**, *69*, 417–423. [[CrossRef](#)]
34. Zhao, J.; Buldum, A.; Han, J.; Lu, J.P. Gas molecule adsorption in carbon nanotubes and nanotube bundles. *Nanotechnology* **2002**, *13*, 195–200. [[CrossRef](#)]
35. Mollaamin, F.; Monajjemi, M. Molecular modelling framework of metal-organic clusters for conserving surfaces: Langmuir sorption through the TD-DFT/ONIOM approach. *Mol. Simul.* **2022**, *49*, 365–376. [[CrossRef](#)]
36. Bakhshi, K.; Mollaamin, F.; Monajjemi, M. Exchange and Correlation Effect of Hydrogen Chemisorption on Nano V(100) Surface: A DFT Study by Generalized Gradient Approximation (GGA). *J. Comput. Theor. Nanosci.* **2011**, *8*, 763–768. [[CrossRef](#)]
37. Mollaamin, F.; Shahriari, S.; Monajjemi, M.; Khalaj, Z. Nanocluster of Aluminum Lattice via Organic Inhibitors Coating: A Study of Freundlich Adsorption. *J. Clust. Sci.* **2022**, 1–16. [[CrossRef](#)]
38. Roderick, A.F.; Kideok, D.K.; Sridhar, K.; James, D.K.; Karl, T.M. Solid-State NMR and Computational Chemistry Study of Mononucleotides Adsorbed to Alumina. *Langmuir* **2006**, *22*, 9281–9286.
39. Yanai, T.; Tew, D.; Handy, N.C. A new hybrid exchange–correlation functional using the Coulomb-attenuating method (CAM-B3LYP). *Chem. Phys. Lett.* **2004**, *393*, 51–57. [[CrossRef](#)]
40. Lehtola, S. A review on non-relativistic, fully numerical electronic structure calculations on atoms and diatomic molecules. *Int. J. Quantum Chem.* **2019**, *119*, e25968. [[CrossRef](#)]
41. Svensson, M.; Humbel, S.; Froese, R.D.J.; Matsubara, T.; Sieber, S.; Morokuma, K. ONIOM: A Multilayered Integrated MO + MM Method for Geometry Optimizations and Single Point Energy Predictions. A Test for Diels–Alder Reactions and Pt(P(*t*-Bu)<sub>3</sub>)<sub>2</sub> + H<sub>2</sub> Oxidative Addition. *J. Phys. Chem.* **1996**, *100*, 19357–19363. [[CrossRef](#)]

42. Brandt, F.; Jacob, C.R. Systematic QM Region Construction in QM/MM Calculations Based on Uncertainty Quantification. *J. Chem. Theory Comput.* **2022**, *18*, 2584–2596. [[CrossRef](#)] [[PubMed](#)]
43. Zhang, C.; Yang, S.; Zhang, X.; Xia, Y.; Li, J. Extended Line Defect Graphene Modified by the Adsorption of Mn Atoms and Its Properties of Adsorbing CH<sub>4</sub>. *Nanomaterials* **2022**, *12*, 697. [[CrossRef](#)] [[PubMed](#)]
44. Becke, A.D. Density-functional thermochemistry. III. The role of exact exchange. *J. Chem. Phys.* **1993**, *98*, 5648–5652. [[CrossRef](#)]
45. Lee, C.; Yang, W.; Parr, R.G. Development of the Colle–Salvetti correlation-energy formula into a functional of the electron density. *Phys. Rev. B* **1988**, *3*, 785–789. [[CrossRef](#)]
46. Ditchfield, R.; Hehre, W.J.; Pople, J.A. Self-consistent molecular-orbital methods. IX. An extended Gaussian-type basis for molecular-orbital studies of organic molecules. *J. Chem. Phys.* **1971**, *54*, 724–728. [[CrossRef](#)]
47. Frisch, M.J.; Trucks, G.W.; Schlegel, H.B.; Scuseria, G.E.; Robb, M.A.; Cheeseman, J.R.; Scalmani, G.; Barone, V.; Petersson, G.A.; Nakatsuji, H.; et al. *Gaussian 16*, Revision C.01; Gaussian, Inc.: Wallingford, CT, USA, 2016.
48. Ciprian, R.; Torelli, P.; Giglia, A.; Gobaut, B.; Ressel, B.; Vinai, G.; Stupar, M.; Caretta, A.; Ninno, G.; Pincelli, T.; et al. New strategy for magnetic gas sensing. *RSC Adv.* **2016**, *6*, 83399–83405. [[CrossRef](#)]
49. Matatagui, D.; Kolokoltsev, O.V.; Qureshi, N.; Mejía-Urriarte, E.V.; Saniger, J.M. A magnonic gas sensor based on magnetic nanoparticles. *Nanoscale* **2015**, *7*, 9607–9613. [[CrossRef](#)]
50. Matatagui, D.; Kolokoltsev, O.V.; Qureshi, N.; Mejía-Urriarte, E.V.; Saniger, J.M. Magnonic sensor array based on magnetic nanoparticles to detect, discriminate and classify toxic gases. *Sens. Actuators B Chem.* **2017**, *240*, 497–502. [[CrossRef](#)]
51. Tahan, A.; Mollaamin, F.; Monajjemi, M. Thermochemistry and NBO analysis of peptide bond: Investigation of basis sets and binding energy. *Russ. J. Phys. Chem. A* **2009**, *83*, 587–597. [[CrossRef](#)]
52. Hsu, S.-C.; Lu, C.; Su, F.; Zeng, W.; Chen, W. Thermodynamics and regeneration studies of CO<sub>2</sub> adsorption on multiwalled carbon nanotubes. *Chem. Eng. Sci.* **2010**, *65*, 1354–1361. [[CrossRef](#)]
53. Kohn, W.; Becke, A.D.; Parr, R.G. Density Functional Theory of Electronic Structure. *J. Phys. Chem.* **1996**, *100*, 12974–12980. [[CrossRef](#)]
54. Parr, R.G.; Pearson, R.G. Absolute hardness: Companion parameter to absolute electronegativity. *J. Am. Chem. Soc.* **1983**, *105*, 7512–7516. [[CrossRef](#)]
55. Politzer, P.; Abu-Awwad, F. A comparative analysis of Hartree-Fock and Kohn-Sham orbital energies. *Theor. Chem. Accounts* **1998**, *99*, 83–87. [[CrossRef](#)]
56. Aihara, J.-I. Reduced HOMO–LUMO Gap as an Index of Kinetic Stability for Polycyclic Aromatic Hydrocarbons. *J. Phys. Chem. A* **1999**, *103*, 7487–7495. [[CrossRef](#)]
57. Silverstein, R.M.; Bassler, G.C. *Spectrometric Identification of Organic Compounds*, 5th ed.; John Wiley & Sons Inc.: Hoboken, NJ, USA, 1981.

**Disclaimer/Publisher’s Note:** The statements, opinions and data contained in all publications are solely those of the individual author(s) and contributor(s) and not of MDPI and/or the editor(s). MDPI and/or the editor(s) disclaim responsibility for any injury to people or property resulting from any ideas, methods, instructions or products referred to in the content.